Trinity College Dublin
Coláiste na Tríonóide, Baile Átha Cliath
The University of Dublin

School of Engineering
Department of Mechanical & Manufacturing Engineering

Sensitivity of the damping controlled fluidelastic instability threshold to mass ratio, pitch ratio and Reynolds number in normal triangular arrays.

Beatriz de Pedro & Craig Meskell

Published in Nuclear Engineering and Design (2018)

CITATION INFORMATION:

"Sensitivity of the damping controlled fluidelastic instability threshold to mass ratio, pitch ratio and Reynolds number in normal triangular arrays." B de Pedro and C. Meskell, Nuclear Engineering and Design 331 (2018) Pages 32–40 doi.org/10.1016/j.nucengdes.2018.02.015

Sensitivity of the damping controlled fluidelastic instability threshold to mass ratio, pitch ratio and Reynolds number in normal triangular arrays.

Beatriz de Pedro Palomar[a], Craig Meskell[b,*]

[a]*School of Engineering, Univeristy of Oviedo, Spain*
[b]*School of Engineering, Trinity College Dublin, Ireland*

Abstract

Sensitivity of the damping controlled fluidelastic instability threshold of normal triangular tube arrays has been investigated through a theoretical-CFD hybrid methodology without the need for experimental data. The quasi-unsteady model with a theoretical model of the memory function was used to predict the critical velocity with the static fluid force coefficients obtained from steady RANS simulations. Five normal triangular tube arrays with pitch to diameter ratios of 1.25, 1.30, 1.32, 1.375 and 1.44 were investigated. Pressure on the tube surface for the $P/d = 1.32$ array, predicted by the CFD, was compared with empirical measurements from the literature. Force coefficients obtained with the validated numerical model, were used to predict stability thresholds for the $P/d = 1.25$ and $P/d = 1.375$ tube arrays and the results were compared with previously published experimental critical velocities. The validated theoretical-CFD hybrid methodology was used to analyze and quantify the critical velocity specific dependence on three parameters: mass ratio, Reynolds number and pitch ratio. As expected, the

*Corresponding author. *E-mail address*: cmeskell@tcd.ie

pitch ratio has the most effect on the critical velocity. It was found that increased Reynolds number increases the stability threshold over the whole range of mass-damping parameters, but mass ratio has only a very minor effect, and this is confined to high mass-damping values.
Keywords:
Fluidelastic Instability, Heat exchanger, Tube arrays

1. Introduction

Flow-induced vibration (FIV) can be a major problem in large heat exchangers leading to shut down or even decommissioning. While turbulent buffeting and the associated wear represents a limit on the long term integrity of these assemblies, fluidelastic instability (FEI) can lead to failure in the short term. As a result, FEI represents a limitation on the operational parameters of the unit. One particular mechanism of FEI, so-called damping controlled instability, can occur when a single flexible tube is subjected to cross flow, even within an otherwise rigid array. It is this mechanism which is the focus of the current study. An exhaustive review of the literature on damping controlled fluidelastic instability in normal triangular tube arrays is beyond the scope of this paper, but a comprehensive introduction to FEI in tube arrays can be found in, for example, Chapter 5 of Paidoussis et al. (2011) and a review of available models for specifically for damping controlled fluidelastic instability is given by Price (1995). Broadly speaking, any of the available models require some experimental input or tuning. For example, even one of the most theoretical the framework proposed by Lever and Weaver (1986) requires the gross flow path between adjacent tubes, and

when it is extended to predict damping controlled instability (Yetisir and Weaver, 1993a) an empirical delay function is necessary.

Previous models of FEI and schemes for collapsing experimental data sets of critical velocity have assumed that the Reynolds number and mass ratio have no effect on levels of critical velocity. However, there is some experimental evidence that this may not be the case (Mewes and Stockmeier, 1991). Price (2001) in his discussion of the applicability of the Connors equation noted that a complete model of FEI should also include a Reynolds number dependency. Mahon and Meskell (2012) have shown that a Reynolds number dependency is necessary to achieve agreement between the Connors type equation and the quasi-steady model. Harran (2014) pointed out the influence of the mass ratio, in an asymptotic approach for the theoretical situation of an undamped structure.

The viability of using CFD, computational fluid dynamics, to obtain non-dimensional force coefficients, as well as other previously empirically determined quantities, and then introduce them into a theoretical framework to obtain stability thresholds, has been investigated by several authors. Hassan et al. (2010) investigated pitch to diameter ratio and Reynolds Number effects on critical velocity for in-line tube arrays by obtaining coefficients for a unsteady the semi-empirical model framework of Chen (1983) from numerical simulations. Khalifa et al. (2013) investigated the interaction between tube vibrations and flow perturbations at lower reduced velocities and Reynolds numbers, coupling numerical predictions of the phase lag and the semi-analytical wavy wall model (Lever and Weaver, 1986; Yetisir and Weaver, 1993a) to predict the reduced critical velocity. Anderson et al. (2014)

developed a model to account for temporal variations in the flow separation for in-line arrays. These types of study offer an interesting alternative to experimental testing which is limited for physical and economical reasons, allowing more extensive investigation of parameter effects in the reduced critical velocity.

This study will use steady CFD calculations of the fluid force coefficients on a displaced tube within an array to predict the critical velocity, using the quasi-unsteady model of Granger and Paidoussis (1996) with the memory function obtained from the wake model proposed by Meskell (2009). The approach is applied to single-phase flow, but it is conceivable that the approach could be adapted to two-phase flow if an appropriate model of two-phase damping is adopted, and an equivalent parameter to Reynolds number could be well defined.

Gillen and Meskell (2009) completed a preliminary study using a similar approach, demonstrating that the scheme was promising. However, that study had significant flaws: the simulations suffered from flow instability in the far wake; only two geometries were simulated; and the range of parameters investigated was small. It is important to note that the objective in this study is not to advance a method of determining the critical velocity *per se*. Rather, the goal of the current study is to investigate the dependence of the critical velocity on mass ratio and Reynolds number.

2. Methodology

Consider a single flexible tube in an otherwise rigid array. It will be assumed that the this tube is free to move only in the transverse direction

(i.e. perpendicular to the mean bulk flow) and that the structure can be represented by a single degree of freedom model. This excludes the possibility of (coupled mode) stiffness controlled instability. In addition, streamwise instability is not possible.

The fluidelastic force E that a tube in an array is subjected to, can be expressed by the governing equation of motion

$$m_s\ddot{y} + c_s\dot{y} + k_s y = F_y(\ddot{y}, \dot{y}, y, U_0) \tag{1}$$

The quantities m_s, c_s and k_s are the structural mass, damping and stiffness respectively. The effects of both turbulent buffeting and vortex shedding have been omitted as it is assumed that they do not change the stability behaviour of this model. This superposition effectively assumes that the dependency of the fluid force on the tube displacement is linear at low amplitudes (i.e. at the onset of instability). Note that if the post-stable behaviour was of interest (i.e. the limit cycle amplitude) then a more sophisticated approach would be needed, but as the focus of this study is the onset of instability, the simplification of a linear relationship with displacement is acceptable. Meskell and Fitzpatrick (2003) demonstrated that the fluidelastic stiffness and damping were cubic in displacement and tube velocity respectively. As a result, the onset of dynamic instability will be governed by the linear parameters. This is generally true in non-linear system dynamics, for example see Chapter 3 of Virgin (2000). Furthermore, these assumptions are widely made in models of fluidelastic instability. For example, Price and Paidoussis (1984) and Lever and Weaver (1986) implicitly assume that the only fluid force is due to tube displacement.

As the full detail of the fluidelastic force function, F_y, is unknown, var-

ious models have been developed. One such model used the quasi-steady approach (Price and Paidoussis, 1984), which assumes the force on the oscillating tube at any moment in time is equal to the force it would experience at that static displacement, but subject to a time lag. This model was later improved upon by Granger and Paidoussis (1996), by replacing the time lag as a function spread over time. In this quasi-unsteady model, the relationship between the instantaneous fluid forces and the static lift and drag force coefficients is

$$F_y(t) = -\frac{1}{2}\rho d^2 L C_M \ddot{y} + \frac{1}{2}\rho U^2 L d(\frac{dC_L}{dy} h * y - C_d \dot{y}) \tag{2}$$

The terms of this equation consist of tube diameter, d, and length, L; the fluid density ρ; freestream velocity, U; and the mass, lift and drag coefficients (C_M, C_L and C_D respectively). The tube displacement y is convolved with the delay function h. The drag, which would normally only be considered for forces in the x direction is included due to the quasi-steady assumption which rotates the fluid force system to be aligned with the instantaneous apparent flow direction. It is worth noting that the strict requirement for the application of the quasi-steady assumption as stated by Van Oudheusden (1995) is that it is possible to "define a steady situation (in which the structure is in rest with regard to some suitably chosen reference frame) which is aerodynamically equivalent to the unsteady situation". But this cannot be met in a tube array because of the proximity of the neighbouring tubes. Nonetheless, it is clear that there should be a positive damping associated with the fluid which will be modified by flow, and so the quasi-steady assumption is included as an imperfect model of this stabilizing effect as its influence is smaller when compared to the influence of the time delayed lift.

The convolution integral can be represented as

$$h * y = \int_0^{\tau} h(\tau - \tau_0) y(\tau_0) d\tau_0 \tag{3}$$

with h representing the memory function

$$h(\tau) = \frac{d\Phi}{d\tau} \tag{4}$$

where $\tau = \frac{tU}{d}$ is the non-dimensional time. The convolution can also be thought of as a low pass filter and so that any response to any vortex shedding and most turbulent excitation will be attenuated, further justifying the assumption in equation 1 to ignore these excitation mechanisms. The transient evolution of this memory function, which is essential for damping controlled FEI, is determined by the function Φ. This transient function converges monotonically towards 1 as τ approaches infinity (Granger and Paidoussis, 1996). Without loss of generality, it can be represented this as a series of decaying exponentials:

$$\Phi = \left(1 - \sum_{i=1}^{N} \alpha_i e^{-\beta_i \tau}\right) H(\tau) \tag{5}$$

Granger and Paidoussis (1996) quantified the parameters α_i and β_i by fitting the model response to experimental data of critical velocity in a normal triangular array subject to cross flow. Li and Mureithi (2016) have quantified these parameters for a parallel triangular array, also by comparison with experimental data, although the main focus of their study was the development of a frequency domain formulation, equivalent to a Theodorsen function. However,Paidoussis et al. (2011) pointed out that using experimental data to determine the detail of the memory function increased the need

for empirical data, largely negating the benefit of a model. Meskell (2009) has proposed a wake model to predict theoretically the values of α_1 and β_1 for a first order model, i.e. $N = 1$ in eqn. 5 .

This wake model approach assumes that the memory function is the normalized instantaneous bound circulation on the tube. The wake is modeled as a discretized vortex sheet. The convection of the shed vorticity is assessed in an idealized velocity field based only on the enforcement of the continuity equation along the gap between tubes. The resulting one dimensional relationship for the temporal variation in lift force on the tube is an integro-differential equation which cannot be solved analytically (Saffman, 1992), but a first order model of the memory function is quantified by numerical quadrature. The non-dimensional values obtained in that study and used here are $\alpha_1 = 1.0$ and $\beta_1 = 0.1572$.

In principle, this approach can be applied to any tube array pattern, but to date, the particular wake model has only been developed for normal triangular arrays. Although it is currently limited to a normal triangular array, this approach has the advantage that no additional experimental data is needed and it does not produce the large overshoots at low non-dimensional time observed in both the fitted memory function of Granger and Paidoussis (1996) or Li and Mureithi (2016).

As the underlying mechanism which gives rises to the memory function is a convection effect, it will have only a weak dependency on Reynolds number if at all. Mahon and Meskell (2013) measured experimentally the time delay associated with the Price and Paidoussis (1984) quasi-steady model (which is closely related to the memory function of the Granger and Paidoussis quasi-

unsteady model used here). They found that the time delay was independent of both Reynolds number and reduced velocity. The effect of Reynolds number will be embedded in the variation of the lift and drag coefficients, which are obtained from steady simulations.

At the critical flow velocity net damping in the coupled system is zero. Practically, the value of the critical flow velocity is obtained by transforming the equation of motion eqn.2 into the Laplace domain by assuming a sinusoidal free response. The resulting characteristic equation is a polynomial, the coefficients of which depend on both the structural parameters and the fluid force parameters, including the flow velocity. The solution of this scalar polynomial is a complex number, with the real part being the frequency of vibration and the imaginary part being the damping. Some manipulation yields yields a quartic polynomial in the critical velocity:

$$\sum_{i=1}^{4} p_i U_c^i = 0 \tag{6}$$

in which $p_i = p_i(\zeta_0, m_r, C_D, \frac{dC_L}{dy}, \alpha_1, \beta_1)$. Derivation of these expressions is tedious, but straight forward. Details can be found in Appendix 1 of Meskell (2009). The only required input data for the model to predict critical velocities are the structural properties ζ_0 (the damping ratio), and m_r (the mass ratio), along with the static fluid force coefficients C_D and $\frac{dC_L}{dy}$. Previously these force coefficients have been obtained via experimental testing. However, in this study these static fluid force coefficients will be determined from numerical simulations.

2.1. Summary of methodology.

The overall hybrid theoretical-CFD model to predict the critical velocity is shown schematically in Fig. 1. For a given tube array pitch ratio a series of steady RANS simulations are conducted to yield the lift and drag coefficients at a range of static tube displacements. The onset flow velocity is changed to vary the Reynolds number. The resulting static fluid force coefficients are then combined with the structural parameters (mass ratio, m_r and structural damping, δ) in the quasi-steady theory proposed by Granger and Paidoussis (1996) using the memory function obtained from the wake model (Meskell, 2009). By solving eqn 6, the resulting hybrid model yields a prediction of the critical velocity which can be assessed for across a range of Reynolds number, mass ratio and pitch ratio, as presented in Section 4.

3. Validation of the hybrid theoretical-CFD model

The aim of the study is to investigate the variation of the critical velocity with mass ratio, pitch ratio and Reynolds number. In order to demonstrate that the hybrid model described in Fig. 1 is appropriate for such an investigation, the approach has been validated at two levels. Firstly, the steady CFD simulation of flow through a deformed array have been compared to experimental surface pressure data. This also facilitated the choice of turbulence model. The second level of validation was achieved by comparing the predicted critical velocity from the entire model to experimental data in the literature. Five normal triangular tube array geometries were considered in this study. In all cases the tube diameter was d=38 mm. Pitch ratios considered were: 1.25, 1.30, 1.32, 1.375 and 1.44. Pitch to diameter ratios

of 1.25, 1.32 and 1.375 were chosen to allow for comparison and validation of the model, as $P/d = 1.32$ was used by Mahon and Meskell (2009) in their surface pressure measurements, while P/d=1.25 and P/d=1.375 were used by Austermann and Popp (1995) in their experimental estimation of critical velocity.

3.1. Computational domain and scheme

The commercial CFD package ANSYS Fluent 12.1 was used to perform steady simulations, using a 2D double precision Reynolds Averaged Navier-Stokes solver, considering a displaced tube in the central position of the third row only. A convergence criteria for residuals of 10^{-5} was necessary to achieve a stable solution. Figure 2 shows a typical velocity magnitude contour plot obtained in these simulations. The flow field is affected by the top and bottom boundaries. This is most obvious in the wake, but flow retardation can also be seen in front of the half tubes. However, in the center of the array the flow field is unaffected.

In order to minimize the effect of the arbitrary constant pressure outlet condition the downstream outlet should be distant from the zone of interest in the array (26th ITTC Specialist Committee on CFD, 2011). However, this space behind the array allows wake oscillations downstream of the array. Note that these oscillations are probably physical rather than numerical artifacts, but they would not be present in a deep array typical of a steam generator. A similar problem was reported by Hassan et al. (2010). In this study the oscillations were suppressed using full-slip guide vans, with negligible thickness which were placed behind each tube gap of the last row. These can be seen in Fig. 2. The flow domain extends $9d$ upstream and down-

stream of the array shown schematically in Figure 3. The inflow condition is a Dirichlet boundary condition on the velocity field, while the outlet is a Dirichlet condition on the pressure field. The top and bottom boundaries are slip walls (i.e. zero shear stress, zero normal velocity). Within the array 200 elements of equal circumferential length were used around each tube. The cells adjacent to the surface have an initial thickness of 0.06 mm and a growth factor of 1.15 until the 13^{th} row of the mesh. This allows the mesh to be deformed to achieve a static displacement, rather than regenerated, and it provides a maximum y^+ value of the order of 1 for all simulations. The near wall mesh is structured quadrilateral, while away from the surface of the tubes the mesh is unstructured triangular. A detail of the mesh between the tubes can be seen in figure 4 . The density and design of the mesh was arrived at after a mesh dependency study. Further details of the computational scheme, the mesh and mesh independence can be found in a related study de Pedro et al. (2016).

3.2. Comparison with experimental surface pressure data

In order to choose an appropriate turbulence model, several simulations were conducted for the $P/d = 1.32$ array, so that the simulated data could be compared directly to the experimental data Mahon and Meskell (2009). This pitch ratio does not exhibit bi-stable flow, and so it is straight forward to compare the experimental surface pressure. The flow conditions and displacement range of the experimental data were matched ($2.1 \times 10^4 \leq Re \leq 1.1 \times 10^5$; $0 \leq \Delta y \leq 0.1d$). Three models were compared: $k - \epsilon$ RNG with non-equilibrium wall function, SST and $k - \omega$. The predicted surface pressure can be reduced to a non-dimensional form:

$$P^* = \frac{P_\theta - P_\theta|_{max}}{P_\theta|_{max} - P_\theta|_{min}} \tag{7}$$

Figure 5 shows the pressure coefficient (Eqn. 7) on the central tube obtained with the three turbulence models and the experimental measurements of Mahon and Meskell (2009), for the particular case of $Re = 2.1 \times 10^4$ and $\Delta y = 0$. Note that θ is defined as zero at the front of the tube. It is clear, that both the SST and the $k - \omega$ models predict substantial asymmetry in the pressure distribution. This is particularly acute in the regions around $\theta = 90^\circ$ and $\theta = 270^\circ$, which are the top and bottom of the tubes. Due to the surface normal direction, these regions will contribute most to the transverse (lift) force and so are of particular concern in estimating the fluid force coefficients for damping controlled fluidelastic instability. This general behaviour was found for all velocities and displacements examined. While it is true that asymmetric flow fields have been observed in tube arrays (Keogh and Meskell, 2015; Mahon and Meskell, 2009, e.g.), it is unlikely that the asymmetry observed in fig. 5 is due to bistable flow for two reasons. Firstly, the numerical model included no-slip guide vanes immediately downstream of the tube array specifically to suppress the large wake structures that give rise to bistable flow inside an array. Secondly, and more importantly, the asymmetric behaviour was observed at all pitch ratios including the lower values. In normal triangular arrays, Mahon and Meskell (2009) did not observe any bistable flow behaviour for $p/d = 1.32$ as shown in fig. 5, but did for $P/d = 1.58$. This would suggest that the asymmetry in the pressure field is an artifact of the numerical scheme.

As a result, the $k - \epsilon$ RNG turbulence model, with non equilibrium func-

tions wall treatment was chosen. This is a pragmatic decision, based on the comparison with experimental pressure data. It is not meant as a recommendation for best practice in modelling flow in tube arrays, nor is it argued that this turbulence model is inherently superior. In fact, it is well known that the $k-\epsilon$ performs poorly for separated flows, and indeed, Fig. 5 clearly shows that this model under-predicts the pressure loss immediately behind the tube. However, as damping controlled FEI is driven largely by lift forces, the poor performance of the other models around the top and bottom of the tube is more important.

Studies of other, quite different, flow systems have also found that a $k-\epsilon$ model may be superior to other turbulence models, in certain circumstances. For example, is a study of heat transfer in a vertical tube Zhang et al. (2017) concluded that the $k-\epsilon$ RNG turbulence model was the best of the 5 models examined. In a comparison of LES and RANS schemes for simulating unsteady flow in inline tube arrays Iacovides et al. (2014) found that the $k-\epsilon$ can give acceptable results. However, it was concluded that the more satisfactory performance was due to to sources of error effectively canceling. This serves to underline the fact that it would be dangerous to claim any generality for using the $k-\epsilon$ RNG with non-equilibrium wall treatment. However, given that the $k-\epsilon$ RNG provides the best comparison to experimental data in this case, it is concluded that it is the most appropriate for the study.

3.3. Comparison with experimental critical velocity data

In order to validate the hybrid theoretical-CFD method, simulations of the $P/d = 1.25$ and $P/d = 1.375$ arrays, matching the experimental setup of Austermann and Popp (1995), were conducted for air in the same Reynolds

number range of laboratory tests, ($2.1 \times 10^4 \leq Re \leq 7.4 \times 10^4$). Using the values for $\frac{dC_L}{dy}$ and C_D obtained from these simulations, the critical velocity was calculated, for the appropriate mass ratio and a structural damping range ($m_r = 493, 0.02 \leq \delta \leq 0.14$).

The comparison between the predictions and the experimental critical velocities (Austermann and Popp, 1995) for the two P/d arrays is shown in Fig. 6. Quantitatively, this methodology consistently under predicts the critical velocity for the $P/d = 1.25$ array, with a relative difference in the range $37\% \rightarrow 62\%$, while for the $P/d = 1.375$ array the relative differences are somewhat lower, within a range of ($0\% \rightarrow 28\%$). There are two possibilities for the deviation. Either the negative fluid damping is over predicted, which is certainly possible given the embedded assumptions of the wake model. Alternatively, the positive fluid damping associated with the drag may be under-predicted. This is very likely as this effect is modeled with the quasi-steady assumption as discussed above. In qualitative terms, the threshold trend was captured for the two arrays. As the study envisioned here is comparative, focused on the trend rather than on the accuracy of the predictions, it is concluded that the approach may be sufficient to conduct the parameter dependency analysis proposed.

4. Sensitivity of the predicted critical velocity to parameter values

It is well known that the pitch ratio effects the critical velocity and has been noted above, there is some evidence in the literature that the critical velocity is also effected by the value of Reynolds number and mass ratio. The

impact of mass ratio is usually bundled into the mass-damping parameter, but this implicitly assumes that damping and mass are equivalent. There may be other non-dimensional numbers that may influence the critical velocity. One candidate might be the Stokes number. The Stokes number posed in terms of the tube diameter is simply the ratio of Reynolds to critical velocity, and as such is a "twice reduced" quantity as Paidoussis et al. (2011) refer to the mass-damping parameter, with the dependent quantity of interest (i.e. the critical velocity) embedded in the parameter being varied. It should be noted that although it is possible to construct a dimensionally correct parameter, it is not clear what length scale or time base should be used. Stokes number finds application in the context of entrainment of particles (e.g. PIV seeding) with the particle size as the length and so may be important in two-phase flow in tube arrays, typical of flow in the center of steam generators. However, this is beyond the scope of the current study, which will focus on the Reynolds number.

Using the hybrid theoretical-CFD method described and validated above, the effect of Reynolds number, mass ratio and pitch ratio ($Re, m_r, P/d$) has been estimated, and the relative importance assessed. Ninety steady simulations, corresponding to the 5 pitch to diameter ratios ($P/d = 1.25, 1.30, 1.32, 1.375, 1.44$), 9 Reynolds numbers ($Re = 10^4 \rightarrow 9 \times 10^4$) and two positions of the displaced tube ($\pm 0.005d$) were carried out. The resulting fluid force coefficients were used in the quasi-unsteady model (Granger and Paidoussis, 1996; Meskell, 2009) with 7 mass ratios and 13 structural damping values. The combination of these parameters produced 8190 stability thresholds estimates. Table 1 summarize the range of variation considered for each parameter in this study.

Parameter	Range
P/d	$(1.25 \rightarrow 1.44)$
Re	$(10^4 \rightarrow 9 \times 10^4)$
m_r	$(10 \rightarrow 10^7)$
δ	$(10^{-9} \rightarrow 10^3)$

Table 1: Parameters range considered in the study of the critical velocity dependency.

4.1. Effect of Reynolds number

The Reynolds number was varied in the steady CFD simulations by almost one order of magnitude from $Re = 10^4$ to $Re = 9 \times 10^4$. This was achieved by changing the onset flow velocity. Figure 7 shows the stability threshold for the 9 Reynolds numbers considered, for a pitch ratio $P/d = 1.375$, and a mass ratio $m_r = 100$. It was found that increased Reynolds number increases the critical velocity over the entire stability threshold, and this effect was seen for all pitch ratios. In the case shown in Fig. 7, increasing the Reynolds number by a factor of 9 resulted in a factor of 1.6 increase in critical velocity at the lowest mass-damping value ($m_r\delta = 10^{-2}$). These results would indicate that the Reynolds number effect is moderate. Furthermore, considering experimental or numerical inputs obtained at low Reynolds numbers in the theoretical models, would yield conservative estimates of critical velocity.

4.2. Effect of mass ratio

The simple time lag embedded in the quasi-steady theory Price and Paidoussis (1984) effectively linearizes the fluid force in time, and so the

mass and damping become combined into a single parameter, the so called mass-damping parameter. This is actually the product of two independent non-dimensional numbers: the mass ratio, m_r and the logarithmic decrement, δ. In the quasi-unsteady model Granger and Paidoussis (1996), the use of a memory function means that the mass and the damping do not always appear together in the governing equation of motion. Thus, the mass-damping parameter does not naturally appear in the coefficients of the characteristic equation (Meskell, 2009). As a result, at a given value of mass-damping, $m_r\delta$, the mass ratio m_r may have a wide range of values. In order to assess the effect of the varying the mass ratio, the critical velocity for the same array as in Fig. 7 was assessed for $10 \leq m_r \leq 10^7$. The higher values of this range are obviously unrealistic (10^4 would be a more realistic upper limit), but this large range was use to achieve a comparable change in critical velocity to that observed for the Reynolds number. Therefore, the first obvious conclusion is that mass ratio is less significant than Reynolds number. However, it is still worth considering if the mass ratio changes the effect of Reynolds number. In order to allow comparison of critical velocities for different Reynolds numbers and mass ratios a renormalized critical velocity can be defined:

$$U_c^* = \frac{U_c}{U_c^{ref}} = \frac{U_c}{U_{c(Re=5\times10^4)}} \tag{8}$$

The reference value is chosen as the critical velocity at $Re = 5 \times 10^4$ as this is the center of the Reynolds number range considered. Note that mass ratio and structural damping are almost fixed for a given tube array installation, but Reynolds number can be varied by the choice of flow velocity. Figure 9 shows the variation of the renormalized critical velocity over a range of Reynolds numbers for increasing mass ratio. The logarithmic decrement

associated with structural damping is $\delta = 0.1$. As can be seen, the effect of increasing Reynolds number is more-or-less linear, but increasing mass ratio increases the sensitivity of critical velocity to Reynolds number: the slope of the trend is steeper for high mass ratio.

Figure 10 shows the effect of varying the structural damping δ with a fixed mass ratio $m_r = 100$. The effect of varying Reynolds number is linear, but again increased damping increases the sensitivity of critical velocity to Reynolds number. However, the degree to which the slope of the trend is changed by increasing damping is not as great. The fact that increasing damping and increasing mass ratio act to move the critical velocity in the same direction suggests that the two parameters can be combined in a single parameter (i.e. the mass-damping parameter), but they are not completely interchangeable, as increased damping has less effect than increased mass ratio and this depends on the value of mass-damping parameter, as already seen in Fig. 7.

In order to show the net effect of increasing the m_r at a constant mass-damping, the behaviour at three mass damping parameters ($m_r\delta = 10^{-2}$, $m_r\delta = 10^4$ and $m_r\delta = 10^4$) were calculated for increasing m_r and decreasing δ and is shown in Fig. 11. For the lowest mass-damping parameter value ($m_r\delta = 10^{-2}$) the variation of the critical velocity with Reynolds numbers shows almost no dependency on mass ratio. As the mass-damping parameter increases, the influence of mass ratio, m_r, becomes stronger.

The range of m_r evaluated was extremely wide, spanning seven orders of magnitude, and yet the effect on critical velocity is modest. Furthermore, looking at Fig. 8, it can be seen that increasing mass ratio does in fact increase

Pitch Ratio, P/d	1.25	1.30	1.32	1.375	1.44
$\frac{\partial C_L}{\partial y}$	-46.23	-21.79	-17.63	-8.023	-4.87
C_D	8.99	6.59	5.89	4.85	3.67

Table 2: Fluid force coefficients for Re=5×10^4

the critical velocity, but this effect is confined to high values of mass-damping parameter. At low values of mass-damping, where the critical velocity will be lowest, the mass ratio has almost no effect. There is theoretical evidence (e.g. Yetisir and Weaver, 1993b) that for high mass-damping values, damping controlled FEI will occur at higher velocities than stiffness controlled FEI, and so this would suggest that the effect of mass ratio might practically be ignored. This explains why the widely adopted pragmatic approach to consider the mass-damping parameter is actually valid, even though the mass ratio and structural damping (logarithmic decrement) are separate physical quantities.

4.3. Effect of pitch ratio

It is well known that pitch ratio is important for the critical velocity. The mechanism for this dependency is that the static fluid force coefficients depend strongly on the pitch ratio, for a given Reynolds number. For example, Table 2 lists the fluid force coefficients obtained from the steady CFD simulations for a Reynolds number of 5×10^4.

The sensitivity of the critical velocity to pitch ratio has been evaluated by considering five pitch ratios: $P/d = 1.25, 1.30, 1.32, 1.375$ and 1.44. In order to compare the behaviour of different pitch ratios at various Reynolds number, the critical velocity was renormalized in a similar way to before. In

this case, the reference value was critical velocity at $P/d = 1.375$, and the particular Reynolds number.

$$U_c^* = \frac{U_c}{U_c^{ref}} = \frac{U_c}{U_{c(P/d=1.375)}} \tag{9}$$

it was found that even after normalization with respect to the reference pitch ratio (1.375), there was still a significant variation due to both Reynolds number and mass-damping parameter. Figure 12 shows the range of normalized critical velocity U_c^* for various pitch ratios over the range of Reynolds numbers ($10^4 \leq Re \leq 9 \times 10^4$). Note that the apparent lack of variation at $P/d = 1.375$ does not mean there is no variation with Reynolds number, but rather that the dataset is referenced to this condition. The mass-damping parameter considered is $m_r\delta = 10$. At the lowest Reynolds number (10^4) the critical velocity for a pitch ratio of 1.25 is only 50% of what would be expected in an array with a pitch ratio of 1.375. In comparison, Chen's empirical correlation Chen (1984) would yield a ratio of 74%. At the highest Reynolds number (9×10^4) for $P/d = 1.44$, the current study predicts a ratio, U_c^* of 120% , while Chen's factor is 114%. The fact that the trend and order of magnitude are similar is encouraging, but there is significant variation associated with Reynolds number. Furthermore, the variation with Reynolds number depends on the mass-damping parameter. For this reason, it has not been practical to develop a simple correction factor which captures the Reynolds number effect, the effect of pitch ratio and the effect of mass-damping.

5. Conclusions

A theoretical-CFD hybrid method has been proposed, in which force coefficients estimated in steady simulations are used as the inputs of the quasi-unsteady model Granger and Paidoussis (1996) and combined with a theoretical memory function Meskell (2009). This allows predictions of critical velocity without the need of any experimental data. Data from the literature was used to validate the CFD simulations and the predictions obtained by the hybrid theoretical-CFD approach. Results of these two comparisons showed reasonable agreement in the pressure distribution in the tube surface and the critical velocity predictions. However, as the discrepancy between the experimental critical velocity and the predicted value is comparable in magnitude to the variations observed, some caution must be exercised. Nonetheless, using this approach the sensitivity of the predictions of critical velocity to values of mass ratio, Reynolds number and pitch ratio was assessed. The main conclusions derived from these studies were:

1. Reynolds number was found to increase levels of critical velocity for the whole stability threshold, by as much as 60 % .
2. While mass ratio has an appreciable effect, it is relatively small, and so it is reasonable to lump the mass ratio and structural damping together in a single parameter, as is commonly done.
3. Pitch ratio was found to have the most significant effect, however, the magnitude of the effect of pitch ratio depends on the Reynolds number.

Although work is need to improve the absolute accuracy of the predictions (for example, with a more sophisticated treatment of the drag in the quasi-

usnteady formulation), the hybrid theoretical-CFD method has yielded some useful insights into damping controlled FEI.

6. Acknowledgment

The authors gratefully acknowledge the financial support of: the Principality of Asturias Government under the PhD grant BP-12054 awarded to Ms. de Pedro.

26th ITTC Specialist Committee on CFD, 2011. Practical guidelines for ship cfd application. ITTC-Recommended Procedures and Guidelines.

Anderson, B., Hassan, M., Mohany, A., 2014. Modelling of fluidelastic instability in a square inline tube array including the boundary layer effect. Journal of Fluids and Structures. 132 (48), 362–375.

Austermann, R., Popp, K., 1995. Stability behaviour of a single flexible cylinder in rigid tube arrays of different geometry subjected to cross-flow. Journal of Fluids and Structures 9 (3), 303 – 322.

Chen, S., 1984. Guidelines for the instability flow velocity of tube arrays in crossflow. Journal of Sound and Vibration 93, 439–455.

Chen, S. S., 1983. Instability mechanisms and stability criteria of a group of circular cylinders subjected to cross-flow. part i: Theory. Journal of Vibrations, Acoustics, Stress, Reliability and Design 105, 51–58.

de Pedro, B., Parrondo, J., Meskell, C., Oro, J., 2016. Cfd modelling of the cross-flow through normal triangular arrays with one tube undergoing

forced vibrations or fluidelastic instability. Journal of Fluids and Structures 64, 67–86.

Gillen, S., Meskell, C., 2009. Numerical analysis of fluidelastic instability in a normal triangular tube array. Proceedings of Flow Induced Vibrations. Prague, Czech Republic.

Granger, S., Paidoussis, M., 1996. An improvement to the quasi-steady model with application to cross-flow-induced vibration of tube arrays. Journal of Fluid Mechanics 320, 163–184.

Harran, G., 2014. Influence of mass ratio on the fluidelastic instability of a flexible cylinder in a bundle of rigid tubes. Journal of Fluids and Structures 47, 71–85.

Hassan, M., Gerber, A., Omar, H., 2010. Numerical estimation of fluidelastic instability in tube arrays. Journal of Pressure and Vessel Technology 132 (4), 041307 (11 pp.) –.

Iacovides, H., Launder, B., West, A., 2014. A comparison and assessment of approaches for modelling flow over. International Journal of Heat and Fluid Flow 49, 69–79.

Keogh, D., Meskell, C., 2015. Bi-stable flow in parallel triangular tube arrays with a pitch-to-diameter ratio of 1.375. Nuclear Engineering and Design 285, 98–108.

Khalifa, A., Weaver, D., Ziada, S., 2013. Modeling of the phase lag causing fluidelastic instability in a parallel triangular tube array. Journal of Fluids and Structures 43, 371–384.

Lever, J., Weaver, D., 1986. On the stability of heat exchanger tube bundles. part i: modified theoretical model. part ii: numerical results and comparison with experiment. Journal of Sound and Vibration 107, 375–410.

Li, H., Mureithi, N., 2016. Development of a time delay formulation for fluidelastic instability model. In: Flow-Induced Vibration and Noise 2016. TNO, pp. 653–662.

Mahon, J., Meskell, C., 2009. Surface pressure distribution survey in normal triangular tube arrays. Journal of Fluids and Structures 25, 1348–1368.

Mahon, J., Meskell, C., 2012. Surface pressure survey in a parallel triangular tube array. Journal or Fluids and Structures 34, 123–137.

Mahon, J., Meskell, C., 2013. Estimation of the time delay associated with damping controlled fluidelastic instability in a normal triangular tube array. Journal of Pressure Vessel Technology, Transactions of the ASME 135 (3).
URL http://dx.doi.org/10.1115/1.4024144

Meskell, C., 2009. A new model for damping controlled fluidelastic instability in heat exchanger tube arrays. Proceedings of the Institution of Mechanical Engineers, Part A: Journal of Power and Energy 223 (4), 361–368.

Meskell, C., Fitzpatrick, J. A., 2003. Investigation of nonlinear behaviour of damping controlled fluidelastic instability in a normal triangular tube array. Journal of Fluids and Structures 18, 573–593.

Mewes, D., Stockmeier, D., 1991. Fluid viscosity effects on flow induced

vibrations of tube bundles in crossflow. In: Flow-induced vibration. I. Mech E. London, pp. 231–242.

Paidoussis, M., Price, S., deLangre, E., 2011. Fuid-Structure Interactions - Cross flow instabilities. Cambridge University Press, Cambridge.

Price, S. J., 1995. A review of theoretical models for fluidelastic instability of cylinder arrays in cross-flow. Journal of Fluids and Structures 9, 463–518.

Price, S. J., 2001. An investigation on the use of connors' equation to predict fluidelastic instability in cylinder arrays. Journal of Pressure Vessel Technology 123, 448–453.

Price, S. J., Paidoussis, M. P., 1984. An improved mathematical model for the stability of cylinder rows subject to cross-flow. Journal of Sound and Vibration 97 (4), 615–640.

Saffman, P. G., 1992. Vortex Dynamics. Cambridge University Press.

Van Oudheusden, B., 1995. On the quasi-steady analysis of one-degree-of-freedom galloping with combined translational and rotational effects. Nonlinear Dynamics 8 (4), 435–451.

Virgin, L. N., 2000. Introduction to experimental nonlinear dynamics : a case study in mechanical vibration". Cambridge Univeristy Press.

Yetisir, M., Weaver, D., 1993a. An unsteady theory for fluidelastic instability in an array of flexible tubes in cross-flow. part i: Theory. Journal of Fluids and Structures 7 (7), 751–766.

Yetisir, M., Weaver, D., 1993b. An unsteady theory for fluidelastic instability in an array of flexible tubes in cross-flow. part ii: Results and comparison with experiments. Journal of Fluids and Structures 7 (7), 767–783.

Zhang, Z., Zhao, C.-R., Yang, X.-T., Jiang, P.-X., Tu, J.-Y., Jiang, S.-Y., 2017. Numerical study of the heat transfer and flow stability of water at supercritical pressures in a vertical tube. Nuclear Engineering and Design 325, 1 – 11.
URL http://dx.doi.org/10.1016/j.nucengdes.2017.09.013

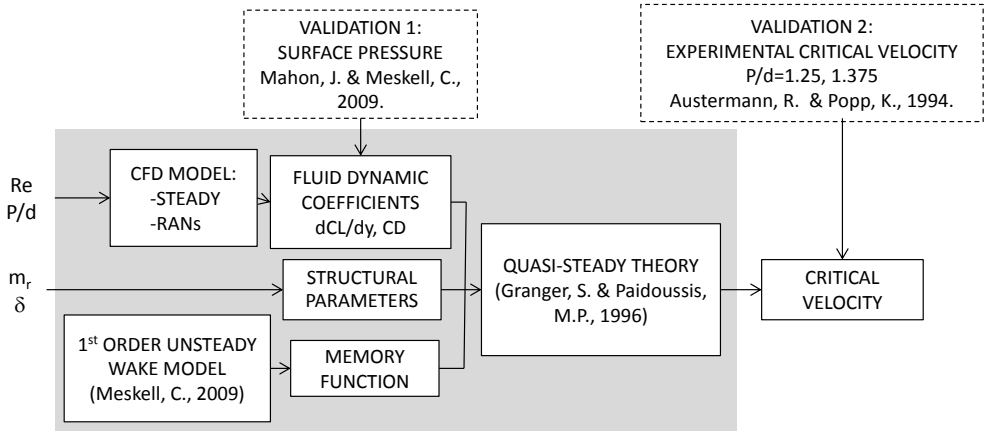

Figure 1: Schematic of the hybrid theoretical-CFD methodology (the grey box).

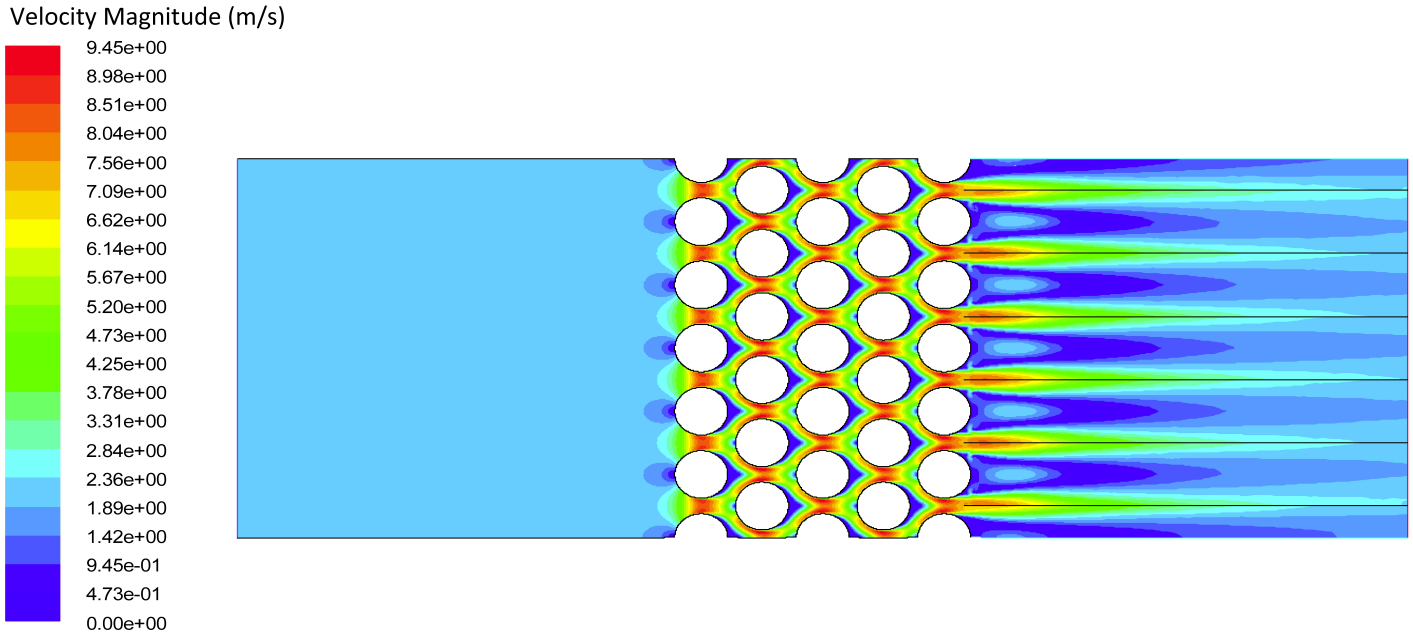

Figure 2: Typical velocity magnitude contours obtained in steady simulations (P/d=1.25, U_0=0.89 m/s).

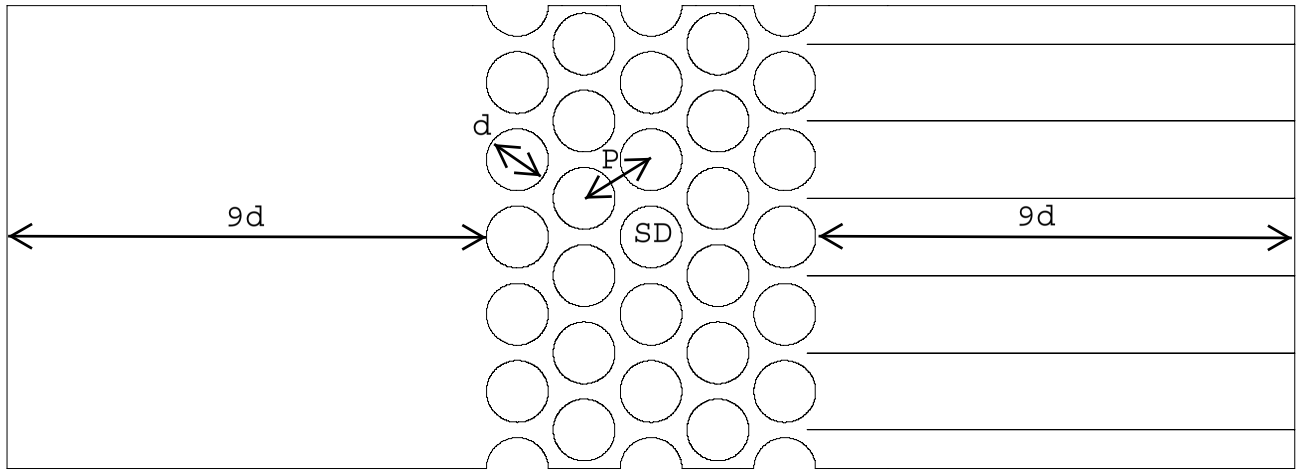

Figure 3: Schematic of computational domain.

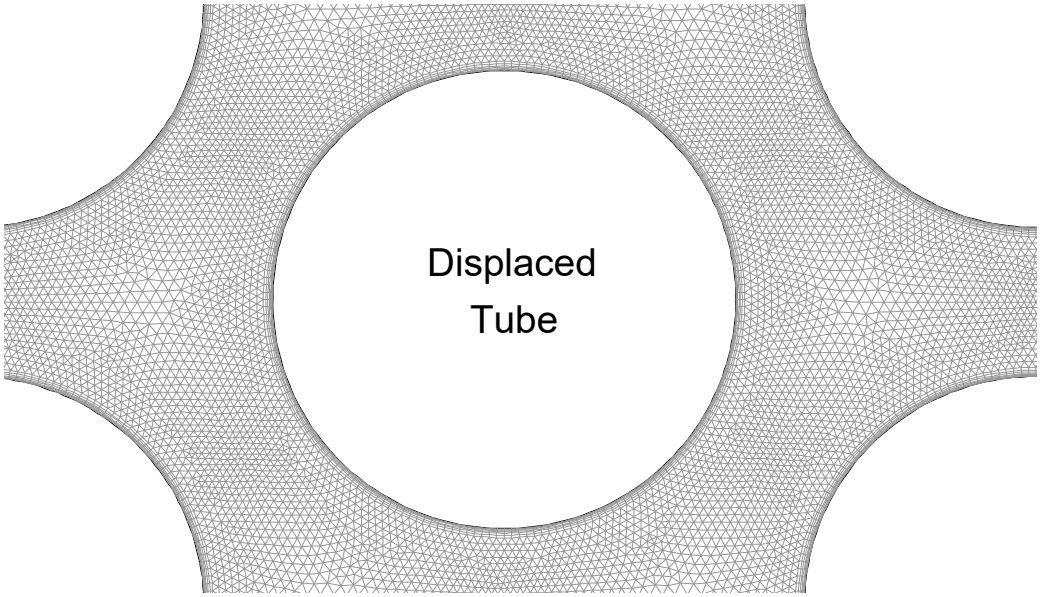

Figure 4: Detail of mesh between tubes.

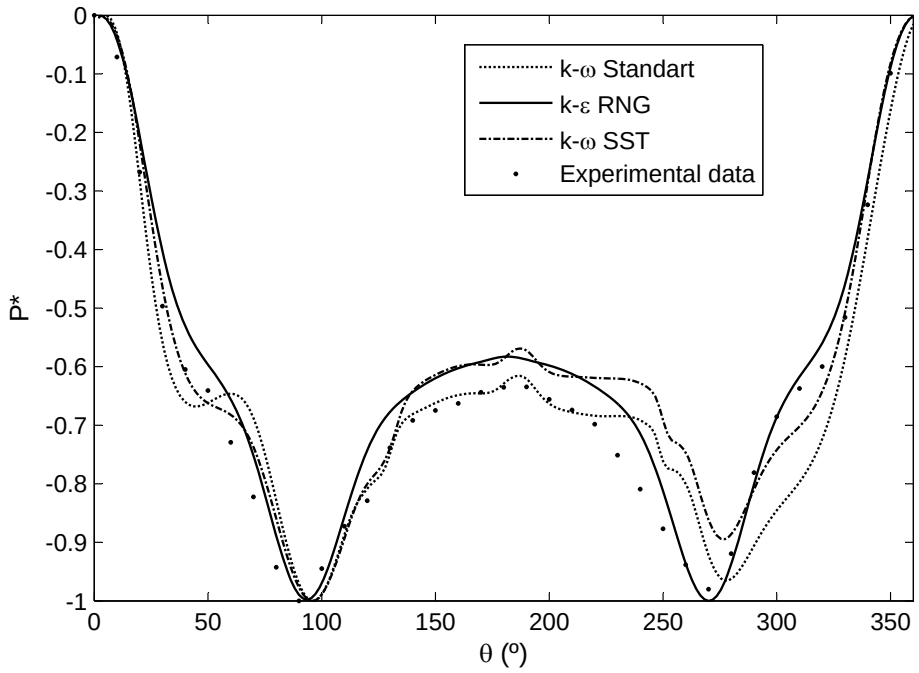

Figure 5: Comparison of pressure coefficient, P^*, on tube surface computed from different turbulence models, with experimental data Mahon and Meskell (2009). $P/d = 1.32$, $Re = 2.1 \times 10^4$ and $\Delta y = 0$.

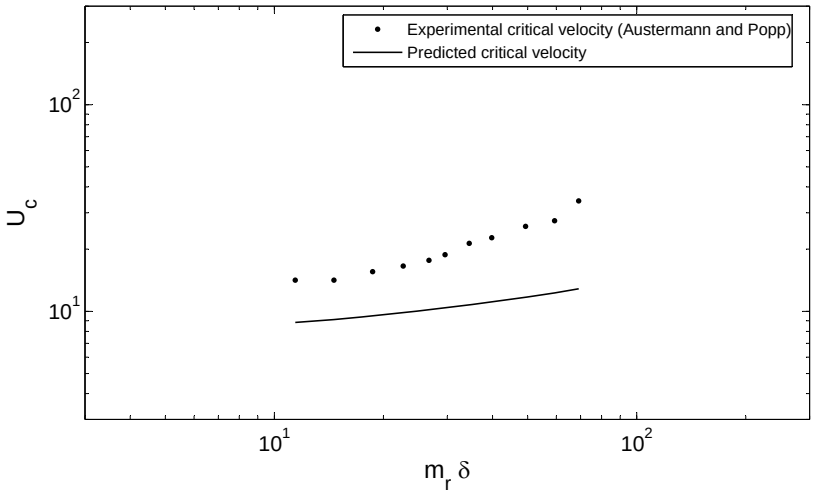

(a) Pitch ratio, P/d=1.25.

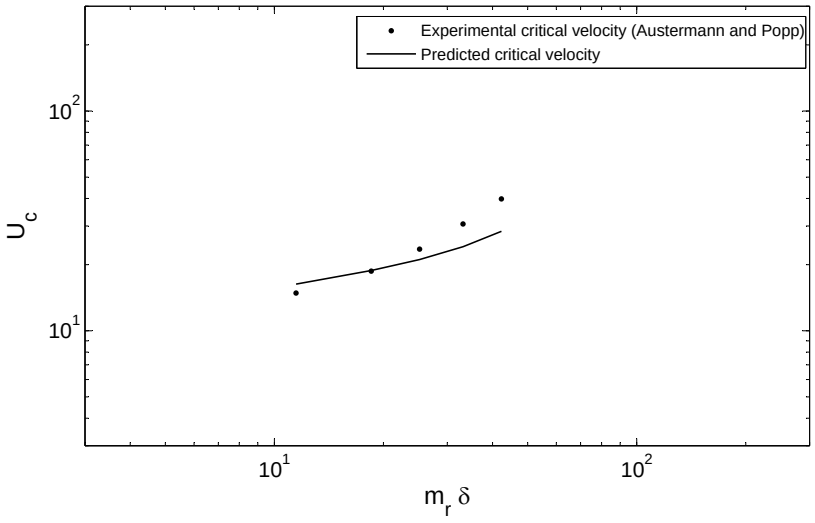

(b) Pitch ratio, P/d=1.375.

Figure 6: Comparison of critical velocity (U_c) predictions with experimental dataAustermann and Popp (1995).

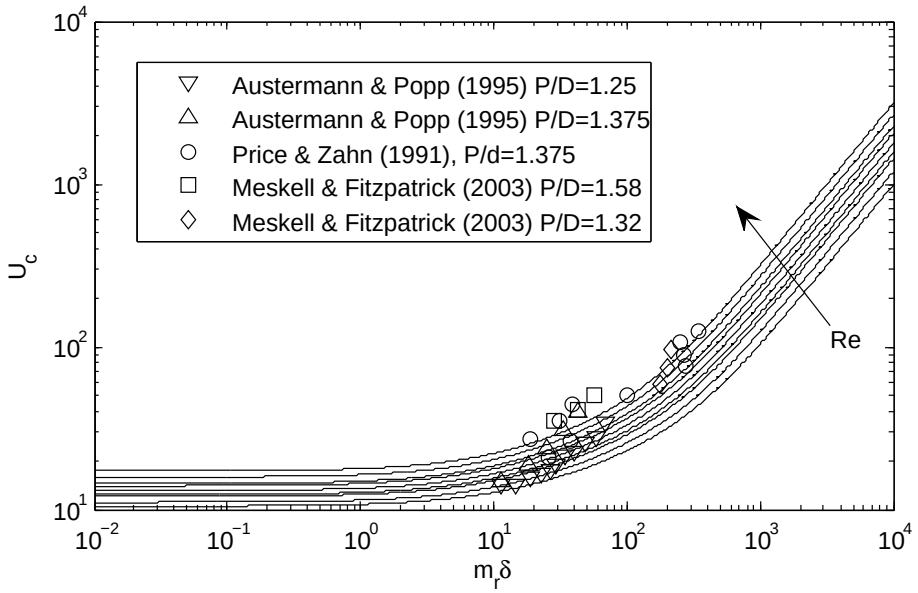

Figure 7: Effect of Reynolds number on the stability threshold, compared with experimental data.

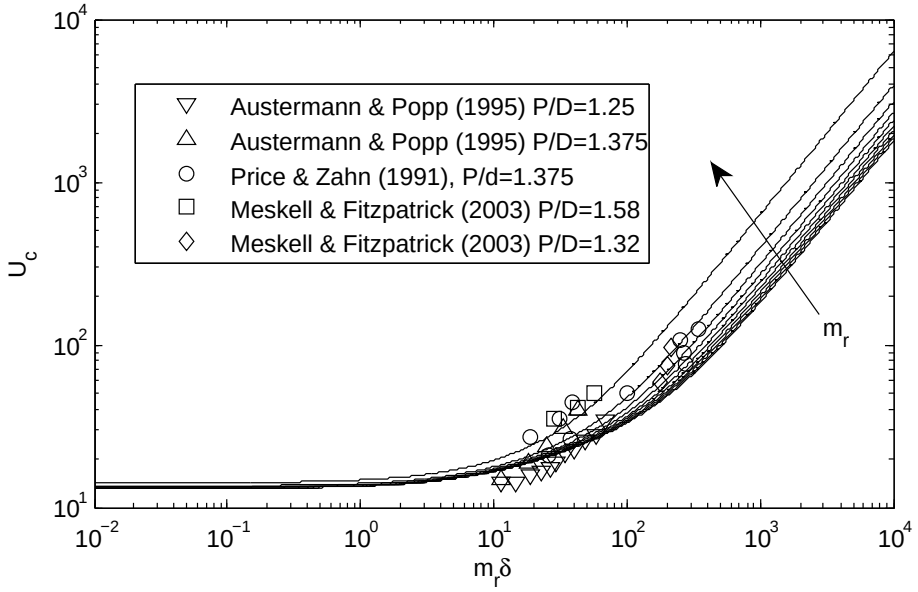

Figure 8: Effect of mass ratio on the stability threshold, compared with experimental data.

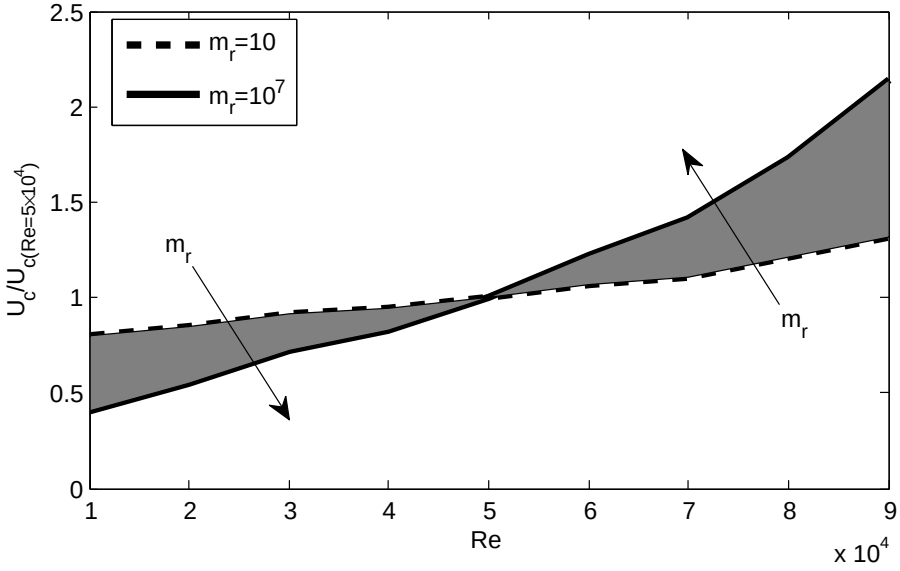

Figure 9: Reynolds number effect on U_c for different m_r values.

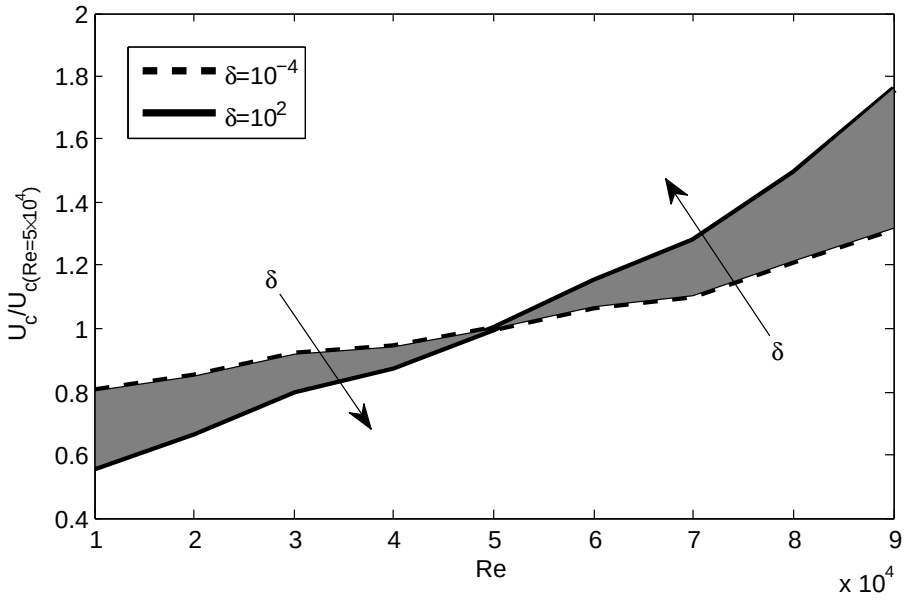

Figure 10: Reynolds number effect on U_c for different δ values.

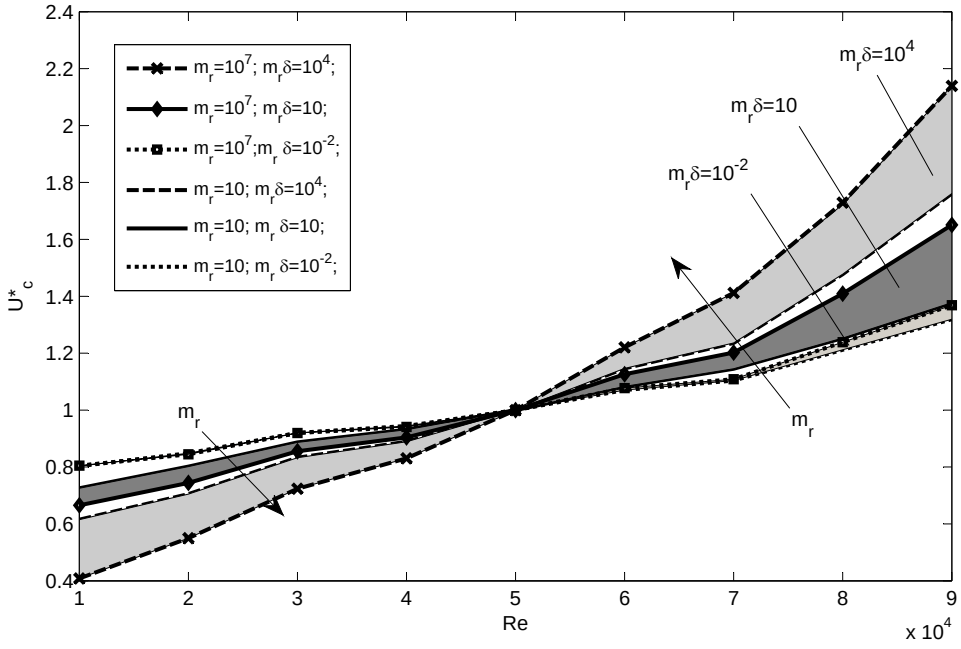

Figure 11: Mass ratio effect on U_c for constant $m_r\delta$.

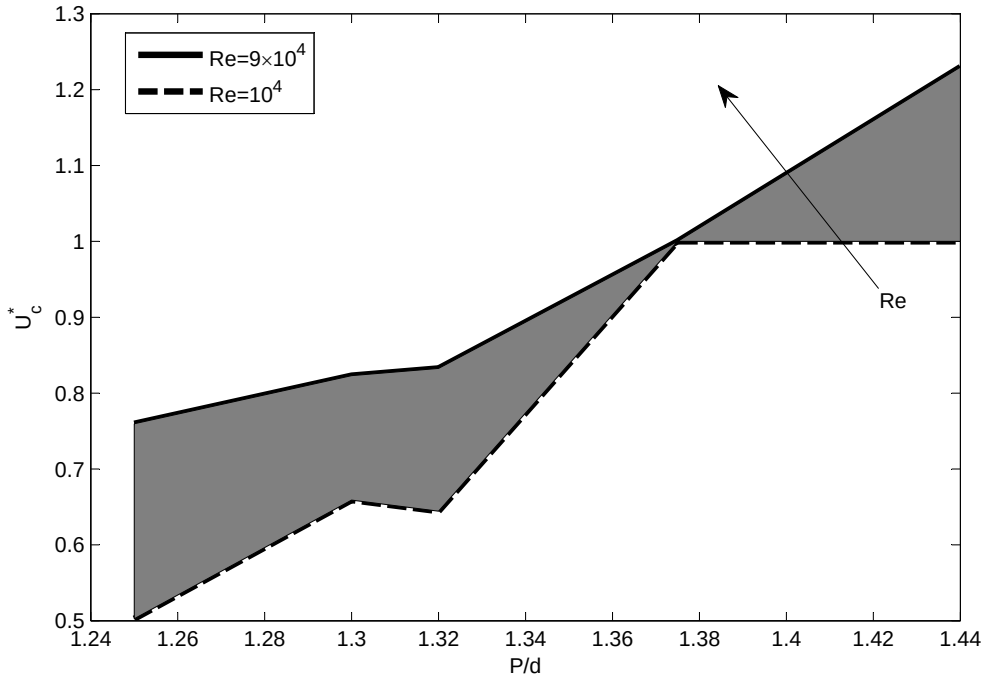

Figure 12: Pitch ratio effect on U_c at different Reynolds numbers ($Re = 10^4 \rightarrow 9 \times 10^4$).